Thermodynamic and Kinetic Study of Carbon Dioxide Hydrogenation on the Metal-Terminated Tantalum-Carbide (111) Surface: A DFT Calculation

Saeedeh Sarabadani Tafreshi [1],*[ID]**, S. Fatemeh. K. S. Panahi** [2]**, Narges Taghizade** [2]**, Maryam Jamaati** [2][ID]**,
Mahkameh Ranjbar** [1] **and Nora H. de Leeuw** [3,4],*[ID]

[1] Department of Chemistry, Amirkabir University of Technology (Tehran Polytechnic),
  No. 350, Hafez Avenue, Tehran 15916-34311, Iran
[2] Department of Physics, Iran University of Science and Technology, Narmak, Tehran 16846-13114, Iran
[3] School of Chemistry, University of Leeds, Leeds LT2 9JT, UK
[4] Department of Earth Sciences, Utrecht University, 3584 CB Utrecht, The Netherlands
[*] Correspondence: s.s.tafreshi@aut.ac.ir (S.S.T.); n.h.deleeuw@leeds.ac.uk (N.H.d.L.)

Abstract: The need to reduce our reliance on fossil fuels and lessen the environmentally harmful effects of CO_2 have encouraged investigations into CO_2 hydrogenation to produce useful products. Transition metal carbides exhibit a high propensity towards CO_2 activation, which makes them promising candidates as suitable catalysts for CO_2 hydrogenation. Here, we have employed calculations based on the density-functional theory to investigate the reaction network for CO_2 hydrogenation to product molecules on the tantalum-terminated TaC (111) surface, including two routes from either HCOOH* or HOCOH* intermediates. Detailed calculations of the reaction energies and energy barriers along multiple potential catalytic pathways, along with the exploration of all intermediates, have shown that CH_4 is the predominant product yielded through a mechanism involving HCOOH, with a total exothermic reaction energy of −4.24 eV, and energy barriers between intermediates ranging from 0.126 eV to 2.224 eV. Other favorable products are CO and CH_3OH, which are also produced via the HCOOH pathway, with total overall reaction energies of −2.55 and −2.10 eV, respectively. Our calculated thermodynamic and kinetic mechanisms that have identified these three predominant products of the CO_2 hydrogenation catalyzed by the TaC (111) surface explain our experimental findings, in which methane, carbon monoxide, and methanol have been observed as the major reaction products.

Keywords: carbon dioxide; hydrogenation; catalyst; tantalum carbide; DFT

1. Introduction

The Earth's expanding population continues to lead to an increase in the world's energy consumption. However, it is now clear that CO_2 emissions from burning fossil fuels [1] are responsible, to a great extent, for climate change and the resulting environmental consequences. Hence, developments in the production of renewable resources and useful products from CO_2 hydrogenation is a fascinating research area [2–4].

Since fossil fuel reserves are finite, hydrogen production and storage as an alternative energy source to balance diminishing oil and gas resources could be feasible in a methanol economy [4,5]. Methanol, an important chemical raw materials, is already in significant demand due to its wide application in power generation and electricity, and it is an excellent alternative fuel [4,6]. Similarly, formic acid is another promising hydrogen storage material, and it is of considerable importance in the chemical and energy industries [2]. Apart from the traditional role of methane (CH_4) for power production and heating, this gas is also valuable for industrial processes and for use in the production of important chemicals, e.g., in its conversion to methanol [1,7]. In addition, the low cost, high purity, versatility, and

variety of chemical reactions for formaldehyde make it a good candidate for use in various industrial applications, especially in the production of resins [8]. It is also considered as a chemical intermediate in many chemical reactions due to its high reactivity [8], and it is one of the final products in carbon dioxide hydrogenation. Carbon monoxide, another product of CO_2 hydrogenation, has also attracted much attention in both academic and industrial settings [9].

As previously mentioned, the conversion of CO_2 into a range of useful products is important, both to achieve sustainable energy and to mitigate its global harmful effects [3,10,11]. Clearly, the design of new efficient, active, and low-cost catalysts to capture, activate, and utilize CO_2 is a major area of research [12,13].

Tantalum carbide, TaC, one of the family of transition metal carbides (TMCs), possesses many of the common characteristics of TMCs, such as extreme hardness, chemical stability, high melting point, and high corrosion resistance [14–17]. Even among the various carbides, TaC is stable at very high temperatures [18,19]. The extraordinary physical and chemical properties of TMCs are attributed to their chemical bond features, which make them a combination of covalent solids and ionic crystals, but with transition metal behavior [20,21]. Although Pt-group metals are valued as highly effective catalysts, their high cost makes them impractical for catalytic processes. Here, it is worth mentioning that TMCs display similar performance to the Pt-group metals, and owing to their low cost, high durability, and high activity, along with their interesting catalytic properties towards many reactions, TMCs are receiving increasing attention [22,23], as originally highlighted by the study by Levy and Boudart in 1973 [24].

Recent experimental and computational studies have confirmed that TMCs can be appealing materials to achieve CO_2 activation [21,22,25–29] and conversion into CO [25], CH_4 [30], CH_3OH [26], as well as other hydrocarbons [31,32]. TMCs show good performance in the reaction of CO_2 conversion, and studies based on the density-functional theory (DFT) have shown that early transition metal carbides (TMCs) such as TiC, ZrC, WC, NbC, TaC, and δ-MoC are able to strongly trap and activate CO_2 [22]. In addition, there is experimental and/or computational evidence that δ-MoC(001), β-Mo_2C (001), α-Mo_2C, WC, metal-terminated NbC(111), and NbC (001) surfaces present high selectivity toward CO_2 conversion [12,25,29,33,34]. In other works, adsorption energies of the CO_2 molecule on the low Miller index (001), (011), and (111) surfaces of TiC and ZrC have been explored, and it was found that CO_2 molecules reduce more easily on the (111) surface than on other facets [35,36].

According to the literature, fcc (111) surfaces of TMCs are less stable and generally more reactive, which is related to the existence of more surface states near the Fermi level than is the case in other low-index surfaces [27,37–39]. The (111) surfaces of TaC have been found to be unreconstructed and terminated by the transition metal after heating and ion or electron bombardment under low-temperature and low pressure conditions [40,41]. Other experimental characterizations of transition metal carbide surfaces have also indicated that the topmost layer of the clean (111) surface consists of metal atoms [14,42]. According to the study by Kitchin et al., TM-terminated carbide surfaces were found to be more reactive than the corresponding pure metal or carbon-terminated carbide surfaces. The surface atoms of the TM-terminated carbide surfaces are under-coordinated compared to the surface atoms of the pure metals, which could explain why atoms and small molecules are adsorbed more strongly, whereas the subsurface carbon atoms are expected to attenuate this effect [15,43]. As such, we have focused our study on the TM-terminated (111) surface, and even though many studies have explored TMC surfaces, there is no comprehensive DFT study regarding CO_2 hydrogenation on the TaC (111) surface. For these reasons, this paper is devoted to the investigation of the physical properties and chemical reactions relevant to the conversion of CO_2 to products on the TaC (111) surface. We have employed calculations based on the density-functional theory to obtain a comprehensive overview of the CO_2 surface chemistry on TaC.

2. Computational Details

2.1. Method

The computational results are obtained using the Vienna Ab initio simulation package (VASP) [44,45], with the exchange-correlation functional developed by Perdew-Burke-Ernzerhof [46] and used within the generalized gradient approximation (GGA). Moreover, in order to improve the energy description of each system, we have included the DFT-D3 dispersion correction, as proposed by Grimme [47], with a plane wave cut-off energy of 600 eV. We have used a Monkhorst–Pack k-point mesh of $11\times11\times11$ and $4\times4\times1$ for the TaC bulk and (111) surface, respectively. The lattice parameter was calculated at $a_0 = 4.450$ Å, which is in excellent agreement with the experimental data ($a_0 = 4.454$ Å) from the inorganic crystal structure database (ICSD) [48] and other DFT studies using different exchange-correlation functionals (4.485 and 4.436 Å) [14]. The convergence force between atoms is set to be smaller than 0.01 eV/Å, and the maximum energy of each atom is converged to 10^{-5} eV. In order to avoid the interaction between neighboring unit cells, a vacuum space of more than 20 Å is introduced to create the surface slabs. Transition states were found using the IDM method [49,50], and frequency calculations were carried out to ensure that we have obtained the correct initial, transition, and final states.

2.2. Model

The TaC (111) surface and the molecules to be adsorbed at the surface are shown in Figure 1. Two possible planes, terminated by tantalum or carbon atoms, exist for the face-centered cubic (fcc) structure of the TaC (111) surface. In this study the tantalum-terminated TaC (111) surface (see Figure 1a) is investigated. To provide an adequate description of the surface relaxations, the TaC (111) surface is constructed of seven layers, with four bottom layers fixed to mimic the bulk crystal. The simulation cell contains 112 atoms and is the same as the slab used in the study by Vojvodic et al. for the adsorption of atoms and molecules on TMC (111) surfaces [51]. Each adsorbed molecule is located in different initial positions on the surface to calculate the favorable adsorption geometries. We have calculated the adsorption energies of the intermediates relative to CO_2 and four H_2 molecules in the gas phase [52]:

$$E_{ads} = E_{C_xO_yH_z}^{surf} + (1-x)E_C^{surf} + (2-y)E_O^{surf} + (8-z)E_H^{surf} - E^{surf} - E_{CO_2}^{gas} - 4*E_{H_2}^{gas} \quad (1)$$

where $E_{C_xO_y}^{surf}$ is the total energy of the C_xO_y intermediates adsorbed on a relaxed TaC (111) surface, and E_C^{surf}, E_H^{surf}, and E_O^{surf} are the energies of isolated carbon, hydrogen, and oxygen atoms, respectively, adsorbed at a distance elsewhere on the relaxed surface. E^{surf}, $E_{CO_2}^{gas}$, and $E_{H_2}^{gas}$ are the energies of the naked TaC (111) slab, isolated gas-phase carbon dioxide, and hydrogen molecules, respectively. Within this definition, a negative E_{ads} value means a release of energy during an exothermic adsorption.
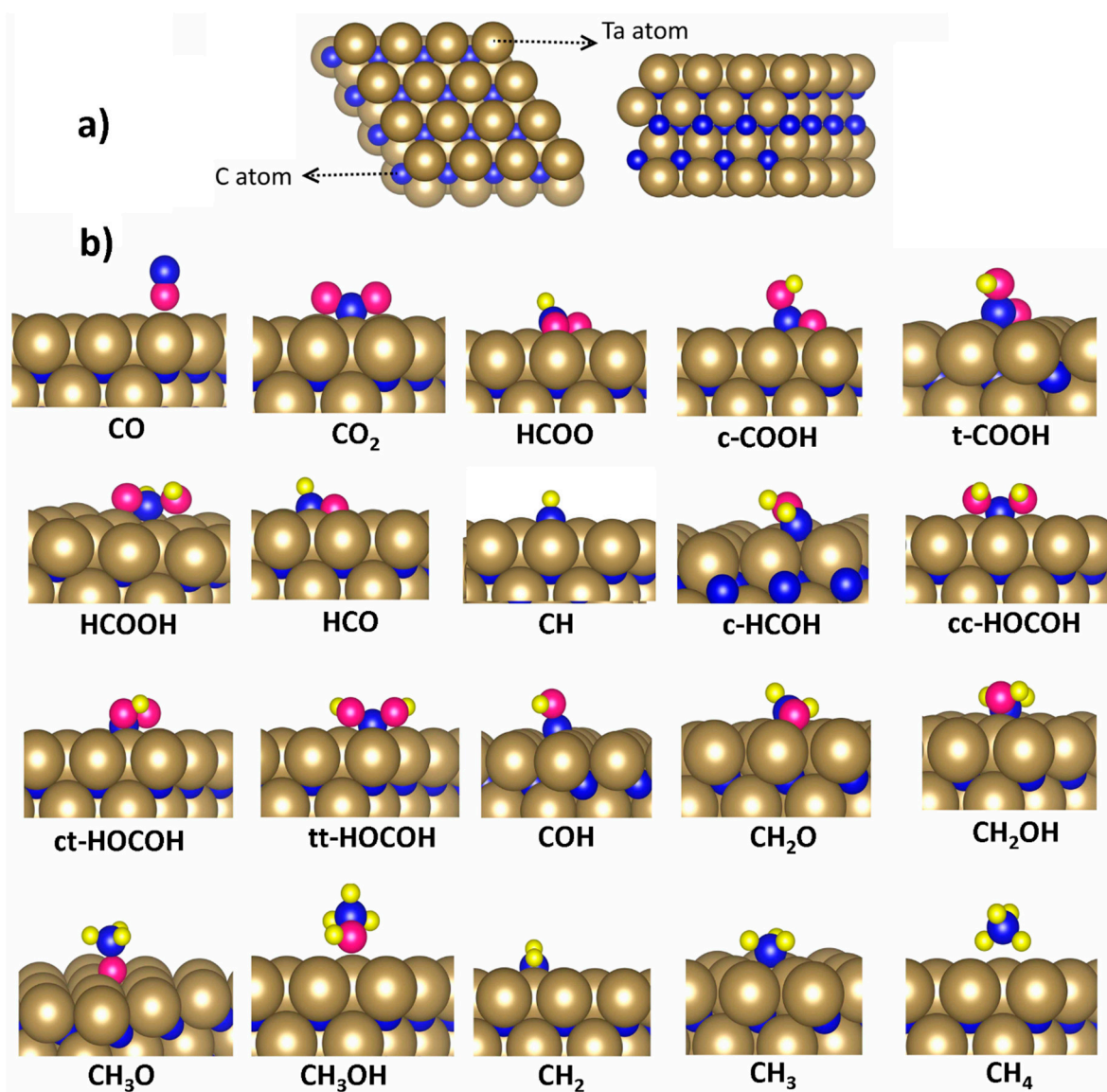
Figure 1. (**a**) TaC (111) surface, (**b**) the adsorbed geometries of the studied species during CO_2 hydrogenation on the TaC (111) surface. Carbon atoms are shown in dark blue, oxygen atoms in magenta, titanium atoms in gold, and hydrogen atoms in yellow spheres.

3. Results and Discussion

3.1. Adsorption Configurations and Energies on TaC (111) Surface

In this section, the CO_2 hydrogenation processes at the TaC (111) surface and the stable adsorption of all possible intermediates are calculated. First, by constructing several initial configurations, the most favorable locations were selected after complete geometric optimization of the TaC (111) surface and adsorbates. The preferred adsorption positions for all intermediates at the TaC (111) surface are presented in Figure 1b, with geometric information and adsorption energies provided in Table 1.

Table 1. The preferred adsorption geometric information and adsorption energies for all intermediates on the TaC (111) surface during CO_2 hydrogenation on the TaC (111) surface.

Species	E_{ads} (eV)	Bond Length (Å)	Species	E_{ads} (eV)	Bond Length (Å)
CO	−0.226	$d*_{Ta-C}$ = 2.27, d_{O-C} = 1.15	c-HCOH	−0.458	$d*_{Ta-O}$ = 2.21, d_{O-C} = 1.51
CO_2	−1.891	$d*_{Ta-O}$ = 2.21, d_{Ta-C} = 2.27	cc-HOCOH	−0.589	$d*_{Ta-O}$ = 2.29, d_{O-C} = 1.45
HCOO	−0.477	$d*_{Ta-O}$ = 2.14, $d*_{Ta-O}$ = 2.27, d_{O-C} = 1.41	ct-HOCOH	−0.739	$d*_{Ta-O}$ = 2.27, d_{O-C} = 1.46
c-COOH	−0.620	$d*_{Ta-O}$ = 2.23, $d*_{Ta-O}$ = 2.22, d_{O-C} = 1.37, d_{O-C} = 1.34	tt-HOCOH	−0.850	$d*_{Ta-O}$ = 2.25, d_{O-C} = 1.46
t-COOH	−0.702	$d*_{Ta-O}$ = 2.21, $d*_{Ta-O}$ = 2.22, d_{O-C} = 1.37, d_{O-C} = 1.34	COH	−0.233	$d*_{Ta-C}$ = 2.05, d_{O-C} = 1.36
HCOOH	−0.711	$d*_{Ta-O}$ = 2.06, d_{O-C} = 1.49, d_{O-C} = 1.35	CH_2O	−0.335	$d*_{Ta-O}$ = 2.20, d_{O-C} = 1.42
HCO	−0.330	$d*_{Ta-O}$ = 2.18, $d*_{Ta-O}$ = 2.18, $d*_{Ta-O}$ = 4.18, d_{O-C} = 1.43	CH_2OH	−0.752	$d*_{Ta-O}$ = 2.23, d_{O-C} = 1.15
CH_2	−0.615	$d*_{Ta-C}$ = 2.23	CH_3O	−0.645	$d*_{Ta-O}$ = 2.24, d_{O-C} = 1.45
CH_3	−0.998	$d*_{Ta-C}$ = 2.42, d_{H-C} = 1.13	CH_3OH	−0.141	$d*_{Ta-O}$ = 2.26, d_{O-C} = 1.45
CH_4	−0.095	d_{Ta-C} = 2.80			

It should be noted that the bond between the molecules and the surface is indicated by the symbol *, while the chemical bonds in each molecule after adsorption are shown without any sign.

CO binds to the TaC (111) surface through its O atom, which is located exactly on top of a surface Ta atom, with a bond length of 2.27 Å and an adsorption energy of −0.226 eV. In the adsorbed CO_2 molecule, two oxygen atoms bond strongly to the surface Ta atoms, while its carbon atom does not bind to the surface atoms; the Ta–O bond lengths are 2.21 Å to both oxygen atoms. Adsorption of the CO_2 molecule results in an alteration in the initial structure of the molecule, where the C–O bond length shortens from 1.177 Å to 1.27 Å. Besides the bond lengths, the O–C–O bond angle decreases from 180° to 132° after adsorption of the molecule, which indicates that the molecule has become activated. These geometric changes have been seen in other studies [53]. For example, the adsorption of CO_2 on the TaC (111) surface without cleavage of the C–O bond agrees with the DFT study of the chemisorption of a CO_2 molecule on the MoC surface, without cleavage of the C–O bonds when the Mo/C ratio is equal to one [54]. The CO_2 adsorption energy (−0.1.891 eV) is also very close to the values found by Kunkel et al. [22,55] for transition metal carbide (001) surfaces.

The adsorption energy of HCOO is −0.477 eV, with a C–O chemical bond of 1.41 Å. Both cis-COOH and trans-COOH approach the surface from their O side, with the oxygen becoming located between the Ta atoms, creating Ta–O bonds of 2.22 and 2.23 Å in c-COOH and 2.21 and 2.22 Å in t-COOH. The adsorption energies of c-COOH and t-COOH are −0.620 eV and −0.702 eV, respectively.

Each oxygen atom of HCOOH bonds to one Ta atom on the surface, with bond lengths of 2.22 Å and 2.23 Å and an adsorption energy of -0.711 eV. The C–O bonds in the HCOOH molecule lengthen by about 9.6% and 11.5% due to adsorption. In the HCO molecule, the oxygen atom is located between three surface Ta atoms, to which it is bound with Ta–O bond lengths of 2.18 Å, 2.18 Å, and 4.18 Å, respectively, causing an adsorption energy of -0.330 eV. Similarly, the O atom of cis-HCOH tends to form a Ta–O bond with a surface Ta atom, with a bond length of 2.21 Å. The c-HCOH molecule is adsorbed immediately above one of the Ta atoms in the surface, with an adsorption energy of -0.458 eV. It is worth mentioning that trans-HCOH on the surface converts to c-HCOH.

Moreover, in the dihydroxycarbene (HOCOH) molecule, the C atom of molecule is located between two surface Ta atoms, but it does not form a bond, whereas two oxygen atoms are bonded with surface Ta atoms with Ta–O bond lengths of 2.29 Å, 2.27 Å, and 2.25 Å and adsorption energies of -0.589, -0.739, and -0.850 eV for cc-HOCOH, ct-HOCOH, and tt-HOCOH, respectively.

The COH molecule approaches the surface by its carbon atom, but the carbon does not bind to the Ta atoms on the surface. The distance between the carbon atom of the CH_2O molecule and a surface Ta atom is 2.05 Å, but it adsorbs via its O atom, with a bond length of 2.20 Å and an adsorption energy of -0.335 eV.

CH_2OH adsorbs on top of a surface Ta site at the TaC (111) through its O atom, with an adsorption energy of -0.752 eV, forming a Ta–O bond length of 2.23 Å and causing the initial C–O bond length to increase by about 10.9%. CH_3O also approaches the surface through its O atom, where the oxygen atom bonds to three surface Ta atoms with equal Ta–O bond lengths of 2.24 Å and an adsorption energy of -0.645 eV. The oxygen atom of CH_3OH adsorbs above a surface Ta atom, with an adsorption energy of just -0.141 eV, forming a Ta–O bond with a bond length of 2.26 Å.

It should be noted that CH_2 prefers to be sited between two surface Ta atoms, but without forming a bond to the TaC (111) surface via its carbon atom. The shortest distance between the C atom and the surface Ta atoms is 2.23 Å, with an adsorption energy of -0.615 eV. CH_3 adsorbs close to the surface in the hollow site of Ta, where it behaves similarly to the CH_2 molecule, at the shortest distance of 2.42 Å between the C atom and the surface Ta atoms and a calculated adsorption energy of -0.998 eV. The CH_4 molecule approaches the surface through its C atom, at a minimum distance of about 2.80 Å and an adsorption energy of -0.095 eV.

3.2. Reaction Networks of CO_2 Hydrogenation

Next, we present a detailed investigation of the reaction networks for all possible intermediates involved in the processes of CO_2 hydrogenation at the Ta-terminated TaC (111) surface. It is known that the TaC (111) surface is able to catalyze the following reactions:

$$CO_2 + 2H \rightarrow CO + H_2O; \tag{2}$$

$$CO_2 + 2H \rightarrow HCOOH; \tag{3}$$

$$CO_2 + 4H \rightarrow CH_2O + H_2O; \tag{4}$$

$$CO_2 + 6H \rightarrow CH_3OH + H_2O; \tag{5}$$

$$CO_2 + 8H \rightarrow CH_4 + 2H_2O \tag{6}$$

Figure 2 explores a range of specific elementary steps for the reaction map of CO_2 hydrogenation to CO, HCOOH, CH_2O, CH_3OH, and CH_4 at the Ta-terminated TaC (111) surface, where the reaction networks include pathways either from HCOO or from (c,t)-COOH.

Figure 2. The possible reaction networks of CO_2 hydrogenation to CO, HCOOH, CH_2O, CH_3OH, and CH_4 at the TaC (111) surface. It should be noted that the adsorbed intermediates on the surface are indicated by the symbol *.

3.3. Chemical Reactions

In this section, we discuss the feasible reactions underpinning the mechanism of CO_2 hydrogenation on the TaC (111) surface. The calculated reaction energies of all intermediates, including the processes of CO_2 hydrogenation at the TaC (111) surface, are shown in Table 2. The initial step associated with CO_2 hydrogenation is either the formation of a formate (HCOO*) or the generation of a carboxyl species (t-COOH* and/or c-COOH*). The former takes place when hydrogen attacks the carbon atom of CO_2 through CO_2* + H* → HCOO*, which requires an energy of 0.198 eV. Similarly, the reactions CO_2* + H* → (c,t)-COOH* occur when H atoms attach to the O atoms of the CO_2 molecule; these are endothermic processes, with energies of 1.056 eV and 0.974 eV for the cis and trans conformer products, respectively. Thus, the first hydrogen atom prefers to attack the carbon atom rather than the oxygen atoms of CO_2 to form HCOO*, which agrees with the results of CO_2 hydrogenation on the bimetallic $MoTiC_2$ MXenes [56]. Formic acid (HCOOH) is generated from the hydrogenation of HCOO* via the reaction HCOO* + H* → HCOOH*, which is also an endothermic process requiring an energy of 1.580 eV. Moreover, further hydrogenation of the carboxyl species can also result in the formation of HCOOH*. These reactions (c,t-COOH* + H* → HCOOH*) are also endothermic processes, with energies of 0.723 eV and 0.805 for the c-COOH* and t-COOH* reactant species, respectively. In

conclusion, the formation of HCOOH* via the carboxyl species is more favorable than via the formate intermediate as a result of the lower reaction energy.

Table 2. The possible reactions and their corresponding energies in the hydrogenation of intermediates to form CO, HCOOH, CH_2O, CH_3OH, and CH_4. It should be noted that the adsorbed intermediates on the surface are indicated by the symbol *.

Elementary Reactions	ΔE (eV)	Elementary Reactions	ΔE (eV)
CO_2 (g) → CO_2*	−1.891	c-COOH* + H* → cc-HOCOH*	1.845
CO_2* + H* → HCOO*	0.198	t-COOH* + H* → tt-HOCOH*	1.666
CO_2* + H* → c-COOH*	1.056	c-COOH* + H* → ct-HOCOH*	1.695
CO_2* + H* → t-COOH*	0.974	t-COOH* + H* → ct-HOCOH*	1.777
c-COOH* → t-COOH*	−0.082	cc-HOCOH* + H* → tt-HOCOH*	−0.261
HCOO* + H* → HCOOH*	1.580	ct-HOCOH* + H* → tt-HOCOH*	−0.111
c-COOH* → CO* + OH*	0.702	tt-HOCOH* → COH* + OH*	−1.375
t-COOH* → CO* + OH*	0.784	ct-HOCOH* → COH* + OH*	−1.486
c-COOH* + H* → HCOOH*	0.723	cc-HOCOH* → COH* + OH*	−1.636
t-COOH* + H* → HCOOH*	0.805	COH* → CO* + H*	0.493
HCOOH* → HCO* + OH*	−1.611	COH* + H* → c-HCOH*	0.589
HCOOH* → HCOOH(g)	2.320	c-HCOH* + H* → CH_2OH*	0.520
HCO* + H* → c-HCOH*	1.687	CH_2OH* + H* → CH_3OH*	1.424
HCO* → CO* + H*	1.590	CH_2OH* → CH_2* + OH*	−1.855
CO* → CO(g)	0.263	CH_2* + H* → CH_3*	0.431
HCO* + H* → CH_2O*	0.809	CH_3* + H* → CH_4*	1.818
CH_2O* → CH_2O(g)	2.834	CH_4* → CH_4 (g)	0.240
CH_2O* + H* → CH_3O*	0.504	CH_3OH* → CH_3OH (g)	1.037
CH_2O* + H* → CH_2OH*	1.398	H_2O* → H_2O (g)	0.894
CH_3O* + H* → CH_3OH*	2.318		

The carboxyl species may further hydrogenate to produce dihydroxycarbene (cc-HOCOH*, ct-HOCOH*, and tt-HOCOH*) through the reaction (c,t)-COOH* + H*→ (ct, cc, tt)-HOCOH*. As is clear from Table 2, all of the above reactions are endothermic processes, although the transformation of (cc,ct)-HOCOH* to tt-HOCOH* is exothermic, with reaction energies of −0.261 eV and −0.111 eV, respectively. Therefore, the reaction pathways for CO_2 hydrogenation at the TaC (111) surface include two routes, either from the HCOOH* or HOCOH* intermediates, which can be followed to achieve the formation of other products. Figure 3. Shows the reaction profile for the hydrogenation of CO_2 and subsequent reactions of intermediates to HCOOH, CO, CH_2O, CH_3OH, and CH_4 via HCOOH, and HOCOH at the TaC (111) surface. In the next section, these reaction pathways are studied in detail.
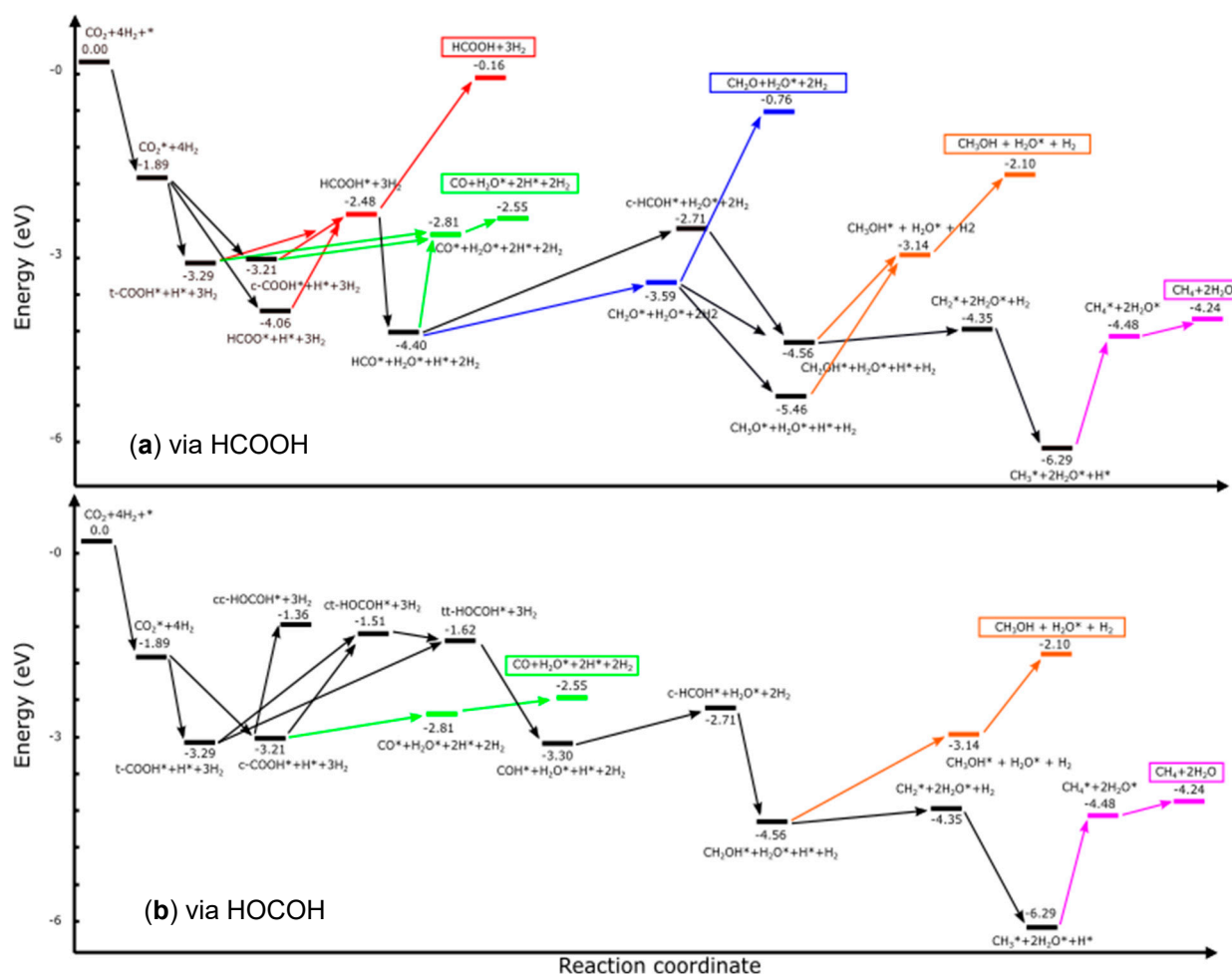
Figure 3. Reaction profile for the hydrogenation of CO_2 and subsequent reactions of intermediates to HCOOH, CO, CH_2O, CH_3OH, and CH_4 via (**a**) HCOOH and (**b**) HOCOH at the TaC (111) surface.

3.3.1. Reaction Pathways of CO_2 to Possible Products through HCOOH

The Reaction Mechanisms for CO_2 Hydrogenation to HCOOH

As discussed above, CO_2 hydrogenation can lead to the formation of HCOO* or the generation of t-COOH* and/or c-COOH*. These species can further react with hydrogen to yield the HCOOH product. Although all these reactions are endothermic processes, the formation of HCOOH* via a carboxyl species appears to be more favorable than via the HCOO* intermediate because of its lower reaction energy.

The Reaction Paths for CO_2 Hydrogenation to CO via HCOOH

There are two paths to CO production: a direct path through the decomposition of (t,c)-COOH* via the reaction (c,t)-COOH* → CO* + OH*, where the reaction is endothermic by 0.702 eV and 0.784 eV for the cis and trans conformers, respectively. Another path is through the decomposition of the HCOOH* intermediate, which leads to the formation of HCO*, with further decomposition of HCO* yielding CO*. The calculated reaction energy of −1.611 eV shows that the decomposition of HCOOH* via HCOOH* → HCO* + OH* is an exothermic process, while the subsequent decomposition of HCO* through HCO* → CO* + H* is an endothermic reaction requiring an energy of 1.590 eV.

The Reaction Paths for the CO_2 Hydrogenation to CH_2O via HCOOH

After formation of HCO*, it can further react with an H atom to form either formaldehyde (CH_2O*) or c-HCOH*. As such, the only pathway to obtain the CH_2O molecule from

CO_2 takes place through the $HCO^* + H^* \rightarrow CH_2O^*$ reaction, with an endothermic energy of 0.809 eV.

The Reaction Paths for CO_2 Hydrogenation to CH_3OH via HCOOH

The pathway to CH_3OH includes either CH_2O^* or c-HCOH*, and these routes are explained separately. As mentioned previously, HCO* hydrogenation can result in the formation of c-HCOH* through $HCO^* + H^* \rightarrow$ c-HCOH*, with a reaction energy of 1.687eV. Next, c-HCOH* attaches a hydrogen via c-HCOH* + $H^* \rightarrow CH_2OH^*$, with an energy of 0.520 eV, to form CH_2OH^*. Further hydrogenation of CH_2OH^* leads to CH_3OH^* (CH_2OH^* + $H^* \rightarrow CH_3OH^*$) which is an endothermic process at an energy of 1.424 eV. The other pathway to CH_3OH is through the hydrogenation of formaldehyde via $CH_2O^* + H^* \rightarrow CH_2OH^*$, which is an endothermic reaction requiring an energy of 1.398 eV. For the subsequent reaction, the CH_2OH^* can further react with another H atom to produce CH_3OH^*, which reaction is endothermic by 1.424 eV. Besides CH_2OH^*, further hydrogenation of CH_2O^* may result in the formation of methoxy (CH_3O^*) via the $CH_2O^* + H^* \rightarrow CH_3O^*$ reaction, which process is endothermic and requires 0.504 eV. Once the formed CH_3O^* intermediate reacts further with another H atom, CH_3OH^* will be produced, with the reaction $CH_3O^* + H^* \rightarrow CH_3OH^*$ requiring 2.318 eV.

The Reaction Paths for CO_2 Hydrogenation to CH_4 via HCOOH

The route to CH_4^* formation involves the dissociation of CH_2OH^* ($CH_2OH^* \rightarrow CH_2^*$ + OH*), which leads to CH_2^*. This reaction is exothermic at −1.855 eV. Next, CH_3^* and CH_4^* are produced through the subsequent hydrogenation of CH_2^* and CH_3^* via CH_2^* + $H^* \rightarrow CH_3^*$ and $CH_3^* + H^* \rightarrow CH_4^*$. Both these reactions are endothermic processes, with reaction energies of 0.431 eV and 1.818 eV, respectively.

3.3.2. Reaction Pathways of CO_2 to Possible Products through HOCOH

As mentioned previously, another route to CO, CH_3OH, and CH_4 products is via the HOCOH* pathway, where HOCOH* conformers form through the hydrogenation of c,t-COOH* via (c,t)-COOH* + $H^* \rightarrow$ (ct, cc, tt)-HOCOH*. The tt-HOCOH* conformer is favored, as conversion of cc-HOCOH* and ct-HOCOH* to tt-HOCOH* ((cc,ct)-HOCOH* + $H^* \rightarrow$ tt-HOCOH*) is exothermic, with energies of −0.261 eV and −0.111 eV, respectively, and tt-HOCOH* is therefore a likely intermediate.

The Reaction Paths for CO_2 Hydrogenation to CO via HOCOH

There are two pathways to CO, directly from (c,t)-COOH* decomposition, where (c,t)-COOH* decomposes to CO* and OH* via the (c,t)-COOH* → CO* + OH* reaction. Both processes are endothermic, with energies of 0.702 eV and 0.784 eV for the cis and trans conformers, respectively. Another pathway involves the decomposition of tt-HOCOH* to COH* and OH* through tt-HOCOH* → COH* + OH*, which is an exothermic reaction by −1.375 eV. Next, CO* will form via further decomposition of COH* via the COH* → CO* + H* reaction, which requires 0.493 eV of energy.

The Reaction Paths for CO_2 Hydrogenation to CH_3OH via HOCOH

Once the formed COH* intermediate reacts further with another hydrogen, c-HCOH* will form through the COH* + $H^* \rightarrow$ c-HCOH* reaction, with an endothermic energy of 0.589 eV. Subsequent hydrogenation of c-HCOH* will produce CH_2OH^* through c-HCOH* + $H^* \rightarrow CH_2OH^*$, which reaction is an endothermic process at 0.520 eV. If CH_2OH^* attaches another hydrogen, CH_3OH^* will finally be produced through the $CH_2OH^* + H^* \rightarrow CH_3OH^*$ reaction, with an endothermic energy of 1.424 eV.

The Reaction Paths for CO_2 Hydrogenation to CH_4 via HOCOH

The dissociation of CH_2OH^* results in CH_2^*, which process takes place through the $CH_2OH^* \rightarrow CH_2^*$ + OH* reaction with an exothermic reaction energy of −1.855 eV. Further

hydrogenation of CH_2^* will produce CH_3^* via $CH_2^* + H^* \rightarrow CH_3^*$, with an energy of 0.431 eV. Finally, subsequent hydrogenation of CH_3^* leads to CH_4^* via $CH_3^* + H^* \rightarrow CH_4^*$, which is also endothermic, at 1.818 eV.

3.4. Activation Energies

In order to gain further insight, activation barriers of a number of selected elementary reactions (listed in Table 3) in the CO_2 hydrogenation process over the TaC (111) surface have been calculated and compared, using the $E_b = E_{TS} - E_{IS}$ relationship, where E_{IS} and E_{TS} represent the total energy of the initial and transition states, respectively. The calculated activation barriers for the selected steps are summarized in Table 3, and in the following section, we will discuss these reactions in more detail, with the initial, transition and final states of the reactions depicted in Figure 4.

Table 3. The selected reactions and their corresponding activation barrier energies. It should be noted that the adsorbed intermediates on the surface are indicated by the symbol *.

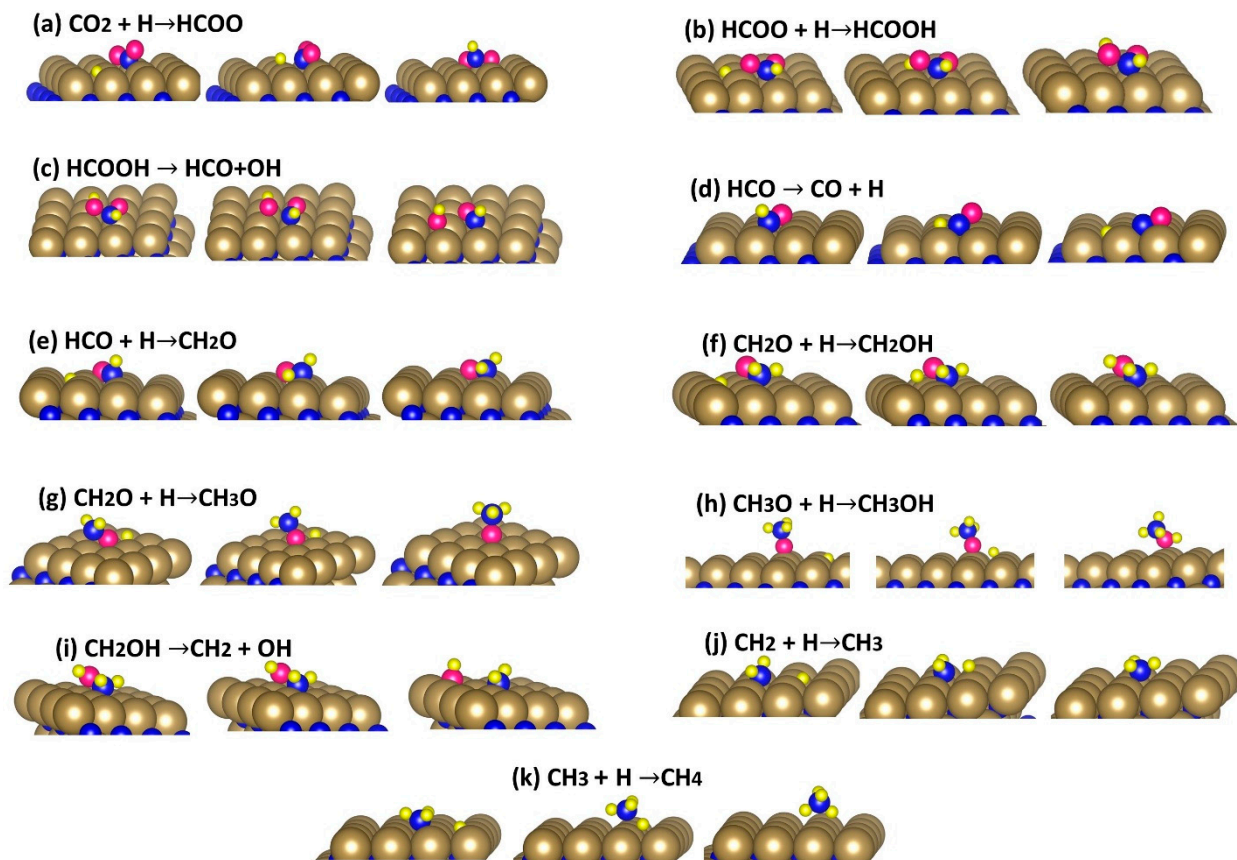| Elementary Reactions	E_b (eV)	Elementary Reactions	E_b (eV)
$CO_2^* + H^* \rightarrow HCOO^*$	0.808	$CH_2O^* + H^* \rightarrow CH_3O^*$	1.282
$HCOO^* + H^* \rightarrow HCOOH^*$	1.828	$CH_3O^* + H^* \rightarrow CH_3OH^*$	1.429
$HCOOH^* \rightarrow HCO^* + OH^*$	0.264	$CH_2OH^* \rightarrow CH_2^* + OH^*$	0.126
$HCO^* \rightarrow CO^* + H^*$	0.614	$CH_2^* + H^* \rightarrow CH_3^*$	1.210
$HCO^* + H^* \rightarrow CH_2O^*$	1.304	$CH_3^* + H^* \rightarrow CH_4^*$	2.224
$CH_2O^* + H^* \rightarrow CH_2OH^*$	1.480		

Figure 4. The selected reactions with their corresponding transition states at the TaC (111) surface.

As previously mentioned, in the formation of HCOO ($CO_2^* + H^* \rightarrow HCOO^*$) H approaches the C atom of CO_2 to form a C–H bond, where the distance between the C and H atoms decreases from 3.29 Å in the initial state (IS) to 1.95 Å in the transition state (TS), and then to 1.10 Å in the final state (FS). The calculated activation barrier is 0.808 eV. The generation of formic acid through formate hydrogenation ($HCOO^* + H^* \rightarrow HCOOH^*$) must overcome an activation barrier of 1.828 eV, where H bonds with the O of formate to form an O–H bond, which shortens from an initial distance of 2.55 Å to 1.27 Å and finally, to 0.98 Å in the IS, TS, and FS, respectively. The dissociation of $HCOOH^*$ via $HCOOH^* \rightarrow HCO^* + OH^*$ has a rather small activation barrier of 0.264 eV, which is therefore kinetically favorable. The increase in the C–O bond length in $HCOOH^*$ weakens the C–O bond, resulting in the decomposition of $HCOOH^*$ to HCO^* and OH^*, with the C–O bond lengthening from 1.49 Å to 1.91 Å and finally, to 3.2 Å in the IS, TS, and FS, respectively. HCO^* can further hydrogenate to formaldehyde or dissociate to carbon monoxide. In the former reaction ($HCO^* + H^* \rightarrow CH_2O^*$), formaldehyde can be produced when the distance between the H* and C atom of HCO^* decreases from 1.61 Å in the TS to 1.15 Å in the FS to form an H–C bond. This reaction must overcome an activation barrier of 1.304 eV. The latter reaction ($HCO^* \rightarrow CO^* + H^*$) takes place over an energy barrier of 0.614 eV, which shows that kinetic CO formation occurs preferentially. The hydrogenation of CH_2O^* generates either CH_2OH^* through $CH_2O^* + H^* \rightarrow CH_2OH^*$ or CH_3O^* via $CH_2O^* + H^* \rightarrow CH_3O^*$. The formation of CH_3O^* (1.282 eV) is slightly more favorable than CH_2OH^* production (1.480 eV), owing to the lower energy barrier.

In the next step, CH_3OH^* can be produced via CH_3O^* hydrogenation ($CH_3O^* + H^* \rightarrow CH_3OH^*$), with an energy barrier of E_b = 1.429 eV. The H atom approaches the O atom of the methoxide, leading to O–H bond formation. In the IS, the distance between H and O is 3.8 Å, decreasing to 1.88 Å and 0.98 Å in the TS and FS, respectively. However, hydroxymethyl (CH_2OH) can dissociate to CH_2^* ($CH_2OH^* \rightarrow CH_2^* + OH^*$), with a small activation barrier of 0.126 eV that is kinetically favorable. The C–O bond in CH_2OH weakens as the bond length increases, from a C-O distance of 1.52 Å to 1.81 Å and 3.18 Å in the IS, TS, and FS, respectively.

As discussed above, CH_2 can be produced from $CH_2OH^* \rightarrow CH_2^* + OH^*$ and then can react further with adsorbed hydrogen to produce CH_4 within two continuous reaction steps. A first pathway to CH_3^* ($CH_2^* + H^* \rightarrow CH_3^*$) has an activation barrier of 1.210 eV, whereas in the subsequent reaction, the adsorbed CH_3 can further react with another H atom to produce CH_4, but with a much higher activation barrier of 2.224 eV. The formed CH_4 species can be assumed to bind only weakly with the surface, from which it may easily desorb.

From the above detailed insight, we can conclude that the mechanism of $CO_2^* \rightarrow HCOO^* \rightarrow HCOOH^* \rightarrow HCO^* \rightarrow CH_2O^* \rightarrow CH_2OH^* \rightarrow CH_2^* \rightarrow CH_3^* \rightarrow CH_4^*$ is the preferred overall exothermic pathway, passing thorough $HCOO^*$ and $HCOOH^*$ species, which releases a total energy of 4.24 eV (Figure 3), indicating that CH_4 is the predominant product of CO_2 hydrogenation over the TaC (111) surface. These results agree well with other studies, showing that all TMCs form CH_4 as the primary product, except for WC and NbC, which produce a significant amount of CO [12]. The rate-determining step (RDS) in this pathway is the hydrogenation reaction of CH_3 to CH_4, with a barrier of 2.224 eV and the largest endothermic reaction energy of 1.818 eV. The smallest barrier, at 0.126 eV, belongs to the reaction of $CH_2OH^* \rightarrow CH_2^* + OH^*$, with the largest exothermic reaction energy of −1.855 eV. The present mechanism resulting in CH_4 formation is also similar to that in the DFT study by Qi et al. [57] on CO hydrogenation over molybdenum carbide, in which they found the same mechanism for the favorable pathway with the reaction of CH_3 to CH_4 as in the RDS reaction. The preferred reaction mechanism is also consistent with previous work studying CO hydrogenation over MoS_2, where the reaction product is CH_4, progressing through the intermediate of CH_2OH prior to C–O bond breaking [58].
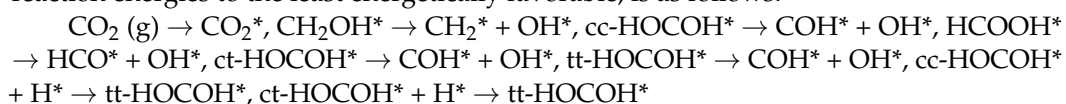
The reaction pathway of $CO_2^* \rightarrow HCOO^* \rightarrow HCOOH^* \rightarrow HCO^* \rightarrow CO^*$ producing CO as the second favored product releases a total energy of 2.55 eV overall. CH_3OH as the next

product was formed by the reaction series $CO_2^* \rightarrow HCOO^* \rightarrow HCOOH^* \rightarrow HCO^* \rightarrow CH_2O^* \rightarrow CH_3O^* \rightarrow CH_3OH^*$, with a total exothermic energy of -2.10 eV. The RDS for the reaction mechanisms resulting in CO and CH_3OH is the hydrogenation step of $HCOO^*$, with a barrier of 1.828 eV, while the reaction of $HCOOH^* \rightarrow HCO^* + OH^*$ contains the smallest barrier of 0.264 eV.

4. Conclusions

We have performed a series of DFT calculations to shed light on the reaction network of CO_2 hydrogenation to CO, HCOOH, H_2CO, CH_4, and CH_3OH products over the Ta-terminated TaC (111) surface, first identifying the optimal adsorption sites for all of the reactants, intermediates, and products on the TaC (111) surface. The adsorption of the CO_2 molecule results in its activation, shown by the alteration of the initial structure, where the C–O bond lengths increase from 1.17 to 1.27 Å and the O–C–O bond angle decreases to 132°. The two oxygen atoms of the CO_2 molecule strongly bond to the Ta atoms on the surface.

The results from the reaction energy calculations of the hydrogenation reaction sequences showed that the largest exothermic reaction energy value of -1.891 eV is related to the adsorption of CO_2^*, which could therefore release sufficient energy to overcome some of the energy barriers in the hydrogenation reactions. The range of exothermic reactions is wide, with the smallest energy of only -0.111eV, produced during the conversion of ct-HOCOH* to tt-HOCOH*. The sequence of reactions, in order of the largest exothermic reaction energies to the least energetically favorable, is as follows:

CO_2 (g) $\rightarrow CO_2^*$, $CH_2OH^* \rightarrow CH_2^* + OH^*$, cc-HOCOH* $\rightarrow COH^* + OH^*$, HCOOH* $\rightarrow HCO^* + OH^*$, ct-HOCOH* $\rightarrow COH^* + OH^*$, tt-HOCOH* $\rightarrow COH^* + OH^*$, cc-HOCOH* $+ H^* \rightarrow$ tt-HOCOH*, ct-HOCOH* $+ H^* \rightarrow$ tt-HOCOH*

The results revealed that the thermodynamically preferred CO_2 hydrogenation mechanism, including two routes from either HCOOH* or HOCOH* intermediates, progresses via $CO_2^* \rightarrow HCOO^* \rightarrow HCOOH^* \rightarrow HCO^*$, which results in CH_4, CO, and CH_3OH formation.

The results from the energy barrier and reaction energy calculations show that the mechanism of $CO_2^* + H^* \rightarrow HCOO^*$, $HCOO^* + H^* \rightarrow HCOOH^*$, $HCOOH^* \rightarrow HCO^* + OH^*$, $HCO^* + H^* \rightarrow CH_2O^*$, $CH_2O^* + H^* \rightarrow CH_2OH^*$, $CH_2OH^* \rightarrow CH_2^* + OH^*$, $CH_2^* + H^* \rightarrow CH_3^*$, and $CH_3^* + H^* \rightarrow CH_4^*$ resulting in methane production is the most exothermic mechanism, releasing a total energy of 4.24 eV, indicating that CH_4 will be the predominant product, which is in good agreement with the results in the available literature. The RDS along this pathway is the hydrogenation reaction of $CH_3^* + H^* \rightarrow CH_4^*$, with a barrier of 2.224 eV and the largest endothermic reaction energy of 1.818 eV, while the dissociation reaction of $CH_2OH^* \rightarrow CH_2^* + OH^*$ has the smallest barrier and largest exothermic reaction energies of 0.126 eV and -1.855 eV, respectively.

Carbon monoxide is the second-most favored product from CO_2 hydrogenation, both thermodynamically and kinetically, through reaction sequences of $CO_2^* + H^* \rightarrow HCOO^*$, $HCOO^* + H^* \rightarrow HCOOH^*$, $HCOOH^* \rightarrow HCO^* + OH^*$, and $HCO^* \rightarrow CO^* + H^*$ and releasing 2.55 eV via the preferred mechanism for CO production. The mentioned mechanism results in CO formation, where $HCOO^* + H^* \rightarrow HCOOH^*$ and $HCOOH^* \rightarrow HCO^* + OH^*$ have the largest and smallest barriers of 1.828 and 0.264 eV, respectively, and the dissociation reactions of $HCOOH^* \rightarrow HCO^* + OH^*$ and $HCO^* \rightarrow CO^* + H^*$ have the largest exothermic and endothermic reaction energies of -1.611 and 1.590 eV, respectively.

Methanol production as the third-preferred product occurs via the reactions of $CO_2^* + H^* \rightarrow HCOO^*$, $HCOO^* + H^* \rightarrow HCOOH^*$, $HCOOH^* \rightarrow HCO^* + OH^*$, $HCO^* + H^* \rightarrow CH_2O^*$, $CH_2O^* + H^* \rightarrow CH_3O^*$, and $CH_3O^* + H^* \rightarrow CH_3OH^*$ by releasing a total exothermic reaction energy of 2.10 eV. Along this pathway, HCOO* hydrogenation and HCOOH* dissociation require the largest and smallest barriers of 1.828 and 0.264 eV, respectively, to be overcome, whereas HCOOH* dissociation and CH_3O^* hydrogenation have the largest exothermic and endothermic reaction energies of -1.611 eV and 2.318 eV, respectively.

The chemical picture and molecular level insights derived from this work suggest that TaC (111) surfaces should have high activity towards CO_2 activation, which along

with their other favorable properties, makes them promising candidates for the catalytic hydrogenation of CO_2 to beneficial products.

References

1. Imyen, T.; Znoutine, E.; Suttipat, D.; Iadrat, P.; Kidkhunthod, P.; Bureekaew, S.; Wattanakit, C. Methane Utilization to Methanol by a Hybrid Zeolite@ Metal–Organic Framework. *ACS Appl. Mater. Interfaces* **2020**, *12*, 23812–23821. [CrossRef] [PubMed]
2. Grasemann, M.; Laurenczy, G. Formic acid as a hydrogen source–recent developments and future trends. *Energy Environ. Sci.* **2012**, *5*, 8171–8181. [CrossRef]
3. Ou, Z.; Qin, C.; Niu, J.; Zhang, L.; Ran, J. A comprehensive DFT study of CO_2 catalytic conversion by H2 over Pt-doped Ni catalysts. *Int. J. Hydrog. Energy* **2019**, *44*, 819–834. [CrossRef]
4. Olah, G.A. Beyond oil and gas: The methanol economy. *Angew. Chem. Int. Ed.* **2005**, *44*, 2636–2639. [CrossRef] [PubMed]
5. Jadhav, S.G.; Vaidya, P.D.; Bhanage, B.M.; Joshi, J.B. Catalytic carbon dioxide hydrogenation to methanol: A review of recent studies. *Chem. Eng. Res. Des.* **2014**, *92*, 2557–2567. [CrossRef]
6. Fiedler, E.; Grossmann, G.; Kersebohm, D.B.; Weiss, G.; Witte, C. Methanol. *Ullmann's Encycl. Ind. Chem.* **2000**, *21*, 611–635.
7. Mostaghimi, A.H.B.; Al-Attas, T.A.; Kibria, M.G.; Siahrostami, S. A review on electrocatalytic oxidation of methane to oxygenates. *J. Mater. Chem. A* **2020**, *8*, 15575–15590. [CrossRef]
8. Gerberich, H.R.; Seaman, G.C. Formaldehyde. *Kirk-Othmer Encycl. Chem. Technol.* **2000**, *11*, 929–951.
9. Zoller, B.; Zapp, J.; Huy, P.H. Rapid Organocatalytic Formation of Carbon Monoxide: Application towards Carbonylative Cross Couplings. *Chem. Eur. J.* **2020**, *26*, 9632.
10. Dzade, N.Y.; de Leeuw, N.H. Activating the FeS (001) surface for CO_2 adsorption and reduction through the formation of sulfur vacancies: A DFT-D3 study. *Catalysts* **2021**, *11*, 127. [CrossRef]
11. Tafreshi, S.S.; Moshfegh, A.Z.; de Leeuw, N.H. Mechanism of Photocatalytic Reduction of CO_2 by Ag3PO4 (111)/g-C3N4 Nanocomposite: A First-Principles Study. *J. Phys. Chem. C* **2019**, *123*, 22191–22201. [CrossRef]
12. Porosoff, M.D.; Kattel, S.; Li, W.; Liu, P.; Chen, J.G. Identifying trends and descriptors for selective CO_2 conversion to CO over transition metal carbides. *Chem. Commun.* **2015**, *51*, 6988–6991. [CrossRef] [PubMed]
13. Bai, S.-T.; De Smet, G.; Liao, Y.; Sun, R.; Zhou, C.; Beller, M.; Maes, B.U.W.; Sels, B.F. Homogeneous and heterogeneous catalysts for hydrogenation of CO_2 to methanol under mild conditions. *Chem. Soc. Rev.* **2021**, *50*, 4259–4298. [CrossRef] [PubMed]
14. Viñes, F.; Sousa, C.; Liu, P.; Rodriguez, J.; Illas, F. A systematic density functional theory study of the electronic structure of bulk and (001) surface of transition-metals carbides. *J. Chem. Phys.* **2005**, *122*, 174709. [CrossRef]
15. Kitchin, J.R.; Nørskov, J.K.; Barteau, M.A.; Chen, J.G. Trends in the chemical properties of early transition metal carbide surfaces: A density functional study. *Catal. Today* **2005**, *105*, 66–73. [CrossRef]
16. Hugosson, H.W.; Eriksson, O.; Jansson, U.; Ruban, A.V.; Souvatzis, P.; Abrikosov, I. Surface energies and work functions of the transition metal carbides. *Surf. Sci.* **2004**, *557*, 243–254. [CrossRef]
17. Sharma, B.I.; Maibam, J.; Paul, R.; Thapa, R.; Singh, R.B. Studies on energy band structure of NbC and NbN using DFT. *Indian J. Phys.* **2010**, *84*, 671–674. [CrossRef]
18. Gilles, R.; Mukherji, D.; Karge, L.; Strunz, P.; Beran, P.; Barbier, B.; Kriele, A.; Hofmann, M.; Eckerlebe, H.; Rösler, J. Stability of TaC precipitates in a Co-Re-based alloy being developed for ultra-high-temperature applications. *J. Appl. Crystallogr.* **2016**, *49*, 1253–1265. [CrossRef]

19. Hocker, S.; Lipp, H.; Schmauder, S.; Bakulin, A.V.; Kulkova, S.E. Ab initio investigation of Co/TaC interfaces. *J. Alloy. Compd.* **2021**, *853*, 156944. [CrossRef]

20. Rodriguez, J.A.; Evans, J.; Feria, L.; Vidal, A.B.; Liu, P.; Nakamura, K.; Illas, F. CO_2 hydrogenation on Au/TiC, Cu/TiC, and Ni/TiC catalysts: Production of CO, methanol, and methane. *J. Catal.* **2013**, *307*, 162–169. [CrossRef]

21. Quesne, M.G.; Roldan, A.; de Leeuw, N.H.; Catlow, C.R.A. Bulk and surface properties of metal carbides: Implications for catalysis. *Phys. Chem. Chem. Phys.* **2018**, *20*, 6905–6916. [CrossRef] [PubMed]

22. Kunkel, C.; Vines, F.; Illas, F. Transition metal carbides as novel materials for CO_2 capture, storage, and activation. *Energy Environ. Sci.* **2016**, *9*, 141–144. [CrossRef]

23. Silveri, F.; Quesne, M.G.; Roldan, A.; De Leeuw, N.H.; Catlow, C.R.A. Hydrogen adsorption on transition metal carbides: A DFT study. *Phys. Chem. Chem. Phys.* **2019**, *21*, 5335–5343. [CrossRef] [PubMed]

24. Levy, R.B.; Boudart, M. Platinum-Like Behavior of Tungsten Carbide in Surface Catalysis. *Science* **1973**, *181*, 547–549. [CrossRef] [PubMed]

25. Liu, X.; Kunkel, C.; Ramírez de la Piscina, P.; Homs, N.; Viñes, F.; Illas, F. Effective and Highly Selective CO Generation from CO_2 Using a Polycrystalline α-Mo2C Catalyst. *ACS Catal.* **2017**, *7*, 4323–4335. [CrossRef]

26. Posada-Pérez, S.; Ramírez, P.J.; Gutiérrez, R.A.; Stacchiola, D.J.; Viñes, F.; Liu, P.; Illas, F.; Rodriguez, J.A. The conversion of CO_2 to methanol on orthorhombic β-Mo 2 C and Cu/β-Mo 2 C catalysts: Mechanism for admetal induced change in the selectivity and activity. *Catal. Sci. Technol.* **2016**, *6*, 6766–6777. [CrossRef]

27. Quesne, M.G.; Roldan, A.; de Leeuw, N.H.; Catlow, C.R.A. Carbon dioxide and water co-adsorption on the low-index surfaces of TiC, VC, ZrC and NbC: A DFT study. *Phys. Chem. Chem. Phys.* **2019**, *21*, 10750–10760. [CrossRef]

28. Posada-Pérez, S.; Ramírez, P.J.; Evans, J.; Viñes, F.; Liu, P.; Illas, F.; Rodriguez, J.A. Highly active Au/δ-MoC and Cu/δ-MoC catalysts for the conversion of CO_2: The metal/C ratio as a key factor defining activity, selectivity, and stability. *J. Am. Chem. Soc.* **2016**, *138*, 8269–8278. [CrossRef]

29. Sarabadani Tafreshi, S.; Ranjbar, M.; Taghizade, N.; Panahi, S.F.K.S.; Jamaati, M.; de Leeuw, N.H. A first-principles study of CO_2 hydrogenation on Niobium-terminated NbC (111) surface. *ChemPhysChem* **2022**, *23*, e202100781. [CrossRef]

30. Xu, W.; Ramírez, P.J.; Stacchiola, D.; Brito, J.L.; Rodriguez, J.A. The Carburization of Transition Metal Molybdates (MxMoO4, M = Cu, Ni or Co) and the Generation of Highly Active Metal/Carbide Catalysts for CO_2 Hydrogenation. *Catal. Lett.* **2015**, *145*, 1365–1373. [CrossRef]

31. Li, N.; Chen, X.; Ong, W.-J.; MacFarlane, D.R.; Zhao, X.; Cheetham, A.K.; Sun, C. Understanding of Electrochemical Mechanisms for CO_2 Capture and Conversion into Hydrocarbon Fuels in Transition-Metal Carbides (MXenes). *ACS Nano* **2017**, *11*, 10825–10833. [CrossRef] [PubMed]

32. Shi, Z.; Yang, H.; Gao, P.; Chen, X.; Liu, H.; Zhong, L.; Wang, H.; Wei, W.; Sun, Y. Effect of alkali metals on the performance of CoCu/TiO₂ catalysts for CO_2 hydrogenation to long-chain hydrocarbons. *Chin. J. Catal.* **2018**, *39*, 1294–1302. [CrossRef]

33. Posada-Pérez, S.; Viñes, F.; Ramirez, P.J.; Vidal, A.B.; Rodriguez, J.A.; Illas, F. The bending machine: CO2 activation and hydrogenation on δ-MoC(001) and β-Mo2C(001) surfaces. *Phys. Chem. Chem. Phys.* **2014**, *16*, 14912–14921. [CrossRef]

34. Porosoff, M.D.; Yang, X.; Boscoboinik, J.A.; Chen, J.G. Molybdenum Carbide as Alternative Catalysts to Precious Metals for Highly Selective Reduction of CO_2 to CO. *Angew. Chem.* **2014**, *126*, 6823–6827. [CrossRef]

35. Morales-García, Á.; Fernández-Fernández, A.; Viñes, F.; Illas, F. CO_2 abatement using two-dimensional MXene carbides. *J. Mater. Chem. A* **2018**, *6*, 3381–3385. [CrossRef]

36. Morales-García, Á.; Mayans-Llorach, M.; Viñes, F.; Illas, F. Thickness biased capture of CO_2 on carbide MXenes. *Phys. Chem. Chem. Phys.* **2019**, *21*, 23136–23142. [CrossRef] [PubMed]

37. Hwu, H.H.; Chen, J.G. Surface Chemistry of Transition Metal Carbides. *Chem. Rev.* **2005**, *105*, 185–212. [CrossRef] [PubMed]

38. Prats, H.; Stamatakis, M. Atomistic and electronic structure of metal clusters supported on transition metal carbides: Implications for catalysis. *J. Mater. Chem. A* **2022**, *10*, 1522–1534. [CrossRef]

39. Johansson, L.I. Electronic and structural properties of transition-metal carbide and nitride surfaces. *Surf. Sci. Rep.* **1995**, *21*, 177–250. [CrossRef]

40. Aizawa, T.; Souda, R.; Otani, S.; Ishizawa, Y.; Oshima, C. Bond softening in monolayer graphite formed on transition-metal carbide surfaces. *Phys. Rev. B* **1990**, *42*, 11469–11478. [CrossRef]

41. Hulbert, S.L.; Kao, C.C.; Garrett, R.F.; Bartynski, R.A.; Yang, S.; Weinert, M.; Jensen, E.; Zehner, D.M. A comparison of the surface electronic structure of Ta(100) and TaC(111) using Auger-photoelectron coincidence spectroscopy. *J. Vac. Sci. Technol. A* **1991**, *9*, 1919–1923. [CrossRef]

42. Zaima, S.; Shibata, Y.; Adachi, H.; Oshima, C.; Otani, S.; Aono, M.; Ishizawa, Y. Atomic chemical composition and reactivity of the TiC(111) surface. *Surf. Sci.* **1985**, *157*, 380–392. [CrossRef]

43. Mavrikakis, M.; Hammer, B.; Nørskov, J.K. Effect of Strain on the Reactivity of Metal Surfaces. *Phys. Rev. Lett.* **1998**, *81*, 2819–2822. [CrossRef]

44. Botana, A.S.; Norman, M.R. Electronic structure and magnetism of transition metal dihalides: Bulk to monolayer. *Phys. Rev. Mater.* **2019**, *3*, 044001. [CrossRef]

45. Kresse, G.; Furthmüller, J. Efficiency of ab-initio total energy calculations for metals and semiconductors using a plane-wave basis set. *Comput. Mater. Sci.* **1996**, *6*, 15–50. [CrossRef]

46. Perdew, J.; Burke, K.; Ernzerhof, M. Perdew, burke, and ernzerhof reply. *Phys. Rev. Lett.* **1998**, *80*, 891. [CrossRef]

47. Grimme, S.; Ehrlich, S.; Goerigk, L. Effect of the damping function in dispersion corrected density functional theory. *J. Comput. Chem.* **2011**, *32*, 1456–1465. [CrossRef]

48. Available online: https://icsd.products.fiz-karlsruhe.de/ (accessed on 3 September 2022).

49. Heyden, A.; Bell, A.T.; Keil, F.J. Efficient methods for finding transition states in chemical reactions: Comparison of improved dimer method and partitioned rational function optimization method. *J. Chem. Phys.* **2005**, *123*, 224101. [CrossRef]

50. Henkelman, G.; Jónsson, H. A dimer method for finding saddle points on high dimensional potential surfaces using only first derivatives. *J. Chem. Phys.* **1999**, *111*, 7010–7022. [CrossRef]

51. Vojvodic, A.; Ruberto, C.; Lundqvist, B.I. Atomic and molecular adsorption on transition-metal carbide (111) surfaces from density-functional theory: A trend study of surface electronic factors. *J. Phys. Condens. Matter* **2010**, *22*, 375504. [CrossRef]

52. Tafreshi, S.S.; Roldan, A.; de Leeuw, N.H. Density functional theory calculations of the hydrazine decomposition mechanism on the planar and stepped Cu(111) surfaces. *Phys. Chem. Chem. Phys.* **2015**, *17*, 21533–21546. [CrossRef]

53. López, M.; Viñes, F.; Nolan, M.; Illas, F. Predicting the Effect of Dopants on CO2 Adsorption in Transition Metal Carbides: Case Study on TiC (001). *J. Phys. Chem. C* **2020**, *124*, 15969–15976. [CrossRef]

54. Xu, W.; Ramirez, P.J.; Stacchiola, D.; Rodriguez, J.A. Synthesis of α-MoC1-x and β-MoCy Catalysts for CO_2 Hydrogenation by Thermal Carburization of Mo-oxide in Hydrocarbon and Hydrogen Mixtures. *Catal. Lett.* **2014**, *144*, 1418–1424. [CrossRef]

55. Kunkel, C.; Viñes, F.; Ramírez, P.J.; Rodriguez, J.A.; Illas, F. Combining Theory and Experiment for Multitechnique Characterization of Activated CO_2 on Transition Metal Carbide (001) Surfaces. *J. Phys. Chem. C* **2019**, *123*, 7567–7576. [CrossRef]

56. Li, Y.; Chen, Y.; Guo, Z.; Tang, C.; Sa, B.; Miao, N.; Zhou, J.; Sun, Z. Breaking the linear scaling relations in MXene catalysts for efficient CO_2 reduction. *Chem. Eng. J.* **2022**, *429*, 132171. [CrossRef]

57. Qi, K.-Z.; Wang, G.-C.; Zheng, W.-J. A first-principles study of CO hydrogenation into methane on molybdenum carbides catalysts. *Surf. Sci.* **2013**, *614*, 53–63. [CrossRef]

58. Shi, X.-R.; Jiao, H.; Hermann, K.; Wang, J. CO hydrogenation reaction on sulfided molybdenum catalysts. *J. Mol. Catal. A Chem.* **2009**, *312*, 7–17. [CrossRef]